Available online at www.sciencedirect.com
SCIENCE DIRECT®
International Journal of Solids and Structures 42 (2005) 4947–4957
INTERNATIONAL JOURNAL OF SOLIDS and STRUCTURES
www.elsevier.com/locate/ijsolstr

Buckling strength analysis of adhesively bonded aluminum hat sections

Jianping Lu *, Golam M. Newaz *, Ronald F. Gibson

Department of Mechanical Engineering, Wayne State University, Detroit, MI 48202, USA

Received 13 October 2004

Abstract

This paper provides an analytical solution for the critical buckling stress of adhesively bonded aluminum hat sections under static axial compression. The governing rectangular plate member of the structure is treated based on the differential equation for out-of-plane deflections of thin plates. Finite element eigenvalue buckling analysis is performed to verify the assumed simply supported boundary conditions for common edges between adjacent plate elements. Elastic restraint is applied to the two loaded edges of the rectangular plate, and the relative critical buckling stress is computed according to the transcendental equations. It is found from experiments that there is no adhesive bonding failure in the elastic buckling stage. The analytical solution yields buckling stress predictions which are in reasonable agreement with measured values.

Keywords: Critical buckling stress; Finite element buckling analysis; Elastic restraint

1. Introduction

Adhesively bonded aluminum hat sections such as the one shown in Fig. 1 present a stiff behavior under axial compression. Their response usually involves very little elastic deformation prior to buckling. Unlike some other structures such as struts whose critical buckling load can be considered as the ultimate load, a thin buckled plate, with four edges simply supported for instance, can carry a much larger load than the critical load at which buckling begins (Timoshenko, 1961). The critical buckling load is, however, an important parameter which characterizes the structure's stability.

* Corresponding authors. Tel.: +1 313 577 5802; fax: +1 313 577 8789 (J. Lu), tel.: +1 313 577 3877; fax: +1 313 577 8789 (G.M. Newaz).
E-mail addresses: ag1751@wayne.edu (J. Lu), gnewaz@eng.wayne.edu (G.M. Newaz).

0020-7683/$ - see front matter © 2004 Elsevier Ltd. All rights reserved.
doi:10.1016/j.ijsolstr.2004.10.018

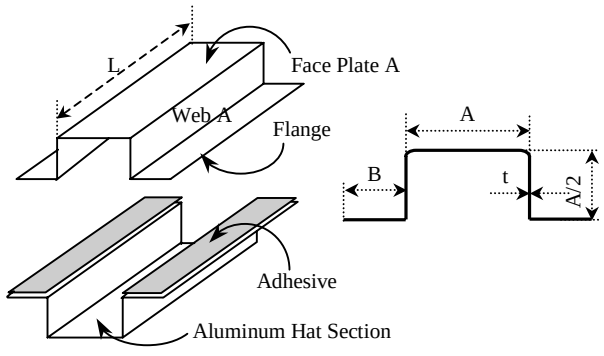

L = 100 mm, A= 50 mm
B = 25 mm, t = 1 mm
Adhesive Layer Thickness: 0.28 mm

Fig. 1. Geometric dimensions of the adhesively bonded aluminum hat section.

The basic governing partial differential equation for out-of-plane problems of thin plates was derived by Saint Venant (1883). Bleich (1952) and Bulson (1969) demonstrated analytically the critical buckling stress solutions for thin rectangular plates with a variety of boundary conditions. More recently, the buckling of a rectangular thin plate with two unloaded edges simply supported and the other two loaded edges elastically restrained was investigated in detail by Plaut and Guran (1994), and the anti-symmetrical buckling mode which was not considered for plates with aspect ratio less than one (Bleich, 1952) was also generally included. Paik and Thayamballi (2000) studied even more complicated cases with all edges elastically restrained, but some approximation had to be made. Peery (1949) pointed out that when a flat plate simply supported at all four edges is loaded by a rigid block, the compression stresses are uniformly distributed along the loading edges if the load is smaller than the buckling load, even though the stresses increase as loading progresses.

Timoshenko (1961) found that when a thin tube of square cross section under uniform compression begins to buckle, there is no bending moments acting between the sides of the buckled tube along the corners, and each side is in the condition of a compressed rectangular plate with simply supported edges. This finding was further extended to a more general case by Bulson (1969) which is that when a number of long flat plates are joined along longitudinal edges to form a thin-walled structural member, the plate elements buckle with common edges of component plates remaining straight. Since there is no involvement of rigid body movement in the elastic buckling analysis, this observation again verified the simply supported boundary conditions described by Timoshenko.

For a given structure, the appropriate plate element has to be separated from the structure and the correct boundary conditions have to be applied, and there is no unified approach to analytically predict the critical buckling load for the entire structure. Becker (1957) proposed an empirical formula to calculate the critical buckling stress of composite hat sections with variable flange/web dimensions. Becker combined all of the geometric factors into a coefficient k, and the values of k were presented in a "k-plate aspect ratio curve". Numerically, some simulation was made to predict the critical buckling load of unstiffened, sandwich and hat-stiffened orthotropic, rectangular plates (Bao et al., 1997), and reasonably accurate simulation of some structures such as pultruded I-beam was also reported (Gan et al., 1999).

The primary purpose of this investigation is to demonstrate a general finite element method of verifying the simply supported boundary conditions for the longitudinal edges in compressively loaded thin-walled structures that may practically have any geometric shapes. Secondly, it is intended to demonstrate by

specially designed experiments that before any analytical evaluation can be made the governing plate element has to be determined by the axial compression test. This is of great importance when the thin-walled structures consist of plate elements with different plate aspect ratios and thicknesses. Finally, this research attempts to demonstrate that a combined analytical/experimental approach can be used to predict the critical buckling stress of any thin-walled structures that are comprised of a number of long flat plates joined along their longitudinal edges.

2. Experiments on axial compression

The materials that were used to build the adhesively bonded aluminum hat sections are Al 6111-T4 aluminum alloy and Dow Betamate® 4601 one part epoxy structural adhesive. To follow the automotive industry practice, no surface preparation was used when the specimens were made. The thickness of the bondline is automatically controlled by the glass beads (0.28 mm in diameter) inside the adhesive. For a thin rectangular plate under compression loading, the edge constraint condition effect on the buckling strength is less obvious with high plate aspect ratio. In order to demonstrate the elastic restraint influence on the buckling strength, a plate aspect ratio of 2 for the face plate shown in Fig. 1 was adopted in this research attempt. The geometrical dimensions of the hat section are shown in Fig. 1. The material properties are listed in Table 1.

Buckling tests were conducted to determine which plate element in the hat section structure is the governing one that buckles first, and as soon as the governing plate buckles, the hat section should be regarded as buckled as well. A special image capture device (shown in Fig. 2) is used to observe simultaneously the buckling of all surfaces with one camera. The compression tests were conducted using a servo-hydraulic MTS machine with an automated data acquisition connected to a time-based medium speed image acquisition system (shown in Fig. 3). The hat section was centered on the bottom test platen, and the lower platen moves up until buckling occurred. Considering the small amount of displacement before buckling, a total of

Table 1
Material properties of aluminum and adhesive

Materials	Young's modulus (GPa)	Poisson's ratio	Yield strength (MPa)
Al 6111-T4 aluminum alloy	69	0.3	175
Betamate® 4601	3.6	0.26	40

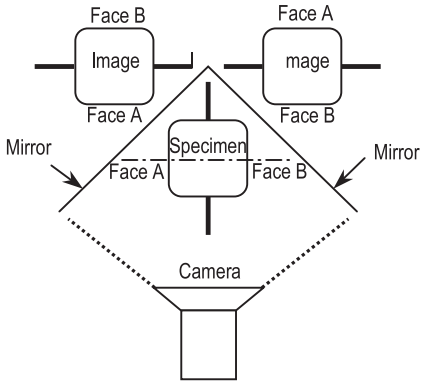

Fig. 2. Image capture device.

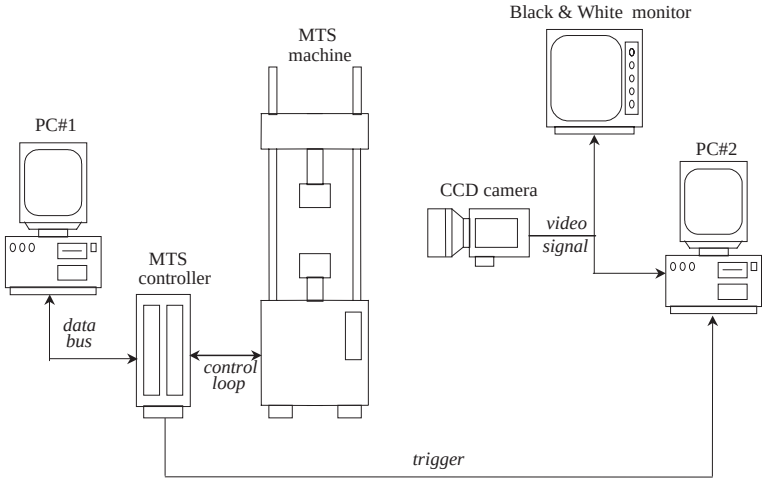

Fig. 3. Compression test MTS system setup.

2 mm axial displacement was set to capture the buckling deformation. The loading rate was 2 mm/min, and 120 images were collected for each test. The images were then analyzed to determine accurately the instant when buckling occurred, and the buckling load was determined from the recorded data accordingly.

3. Finite element eigenvalue buckling analysis

Due to the difficulty in experimentally determining the boundary conditions for the common edges of the buckled plate elements, numerical analysis was performed to investigate the deformation patterns at these edges when buckling occurs.

The eigenvalue buckling analysis was carried out using the ABAQUS code. In the finite element context, the classical eigenvalue buckling problem may be stated as follows. Given a structure with an elastic stiffness matrix, $K^{NM}_{(b)}$, a loading pattern defined by the vector Q^M, and an initial stress and load stiffness matrix, $K^{NM}_{(Q)}$, find load multipliers (eigenvalues), λ_i, and buckling mode shapes (eigenvectors), ϕ^M_i, which satisfy

$$[K^{NM}_{(b)} + \lambda_i K^{NM}_{(Q)}]\phi^M_i = 0 \tag{1}$$

The critical buckling loads are then given by $\lambda_i Q^M$.

In Eq. (1), the superscripts N and M change from 1 to the degree of freedom of the whole model, and the subscript i refers to the ith buckling mode.

The hat section was modeled by 2400 S4R shell elements as shown in Fig. 4, and the adhesive material was also included in the model by use of the special "Sandwich" shell element design in ABAQUS. Elastic restraint was implemented by using a group of rotational spring elements on both ends of the hat section model as shown in Fig. 5. In order to generally verify the simply supported boundary condition of the common edge between plate elements, such as the edge between face A and web A in Fig. 1, the out-of-plane deflection of this common edge was examined in two different practical loading cases that have torsional spring constants $K = 2500$ (N m/rad) and $K = 50{,}000$ (N m/rad) respectively on both ends of the hat section.

In general, if the elastic restraint on both ends of the hat section is lower than a certain value, the face plate would buckle into an anti-symmetric mode rather than a symmetric mode. This is due to the fact that

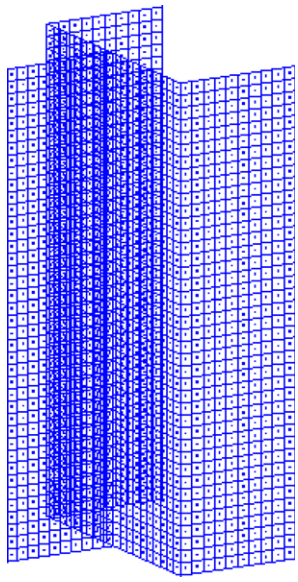

Fig. 4. Finite element model of adhesively bonded aluminum hat section.

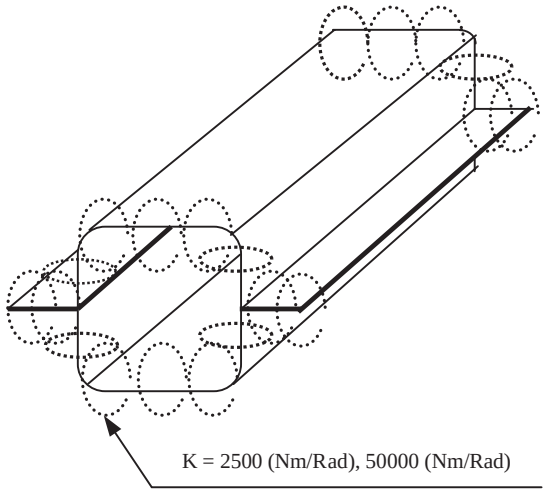

Fig. 5. Elastic restraint represented by a group of rotational spring elements.

there is not enough restraint on the edge of the loading end to provide a greater moment than is required by the symmetric mode. Since it is technically difficult to measure the elastic restraint on the loading ends of the hat section, and the experiment showed a symmetric buckling mode on the face plate, the torsional spring constant that is used in the computational simulation has to be selected in such a way that the symmetric buckling mode is present in the simulation. Because the above selected torsional spring constants $K = 2500$ (N m/rad) and $K = 50{,}000$ (N m/rad) both represent the symmetric buckling mode in the longitudinal direction, it is intended to demonstrate that the assumed simply supported boundary condition is correct in a wide range of elastic restraint levels.

Theoretically, the torsional spring constant on both ends of the hat section has to be infinite to represent the completely fixed condition. Since the ends of the hat section are not completely fixed but elastically restrained by the loading platen, a certain value has to be used for numerical calculation, and this value has to yield a symmetric buckling mode in the result. The buckling mode for $K = 50{,}000$ (N m/rad) is very close to the pure symmetric shape while $K = 2500$ (N m/rad) is somewhere in the very early transition from a symmetric to an anti-symmetric buckling mode.

In the finite element modeling, there is no user applied boundary conditions on the common edge between the face and the web plate elements, and all the nodes on the common edge have all six degrees of freedom. After the simulation, the degree of freedom that represents the out-of-plane displacement of the face plate should be examined and compared with that of the centerline of the face plate. If the out-of-plane displacement level is negligible compared to the centerline values, the face plate can then be regarded as simply supported.

4. Critical buckling stress analysis

To calculate analytically the critical buckling stress of the rectangular plate, for example face A in Fig. 1, the boundary conditions on all the four edges are required to solve the thin plate partial differential equation. Finite element analysis results verified the simply supported condition for the two unloaded edges. The other two loaded edges should be regarded as elastically restrained due to the restraining web plates and surface contact with the platen of the MTS machine. Even though Bleich (1952) derived a formula to calculate the non-dimensional coefficient of restraint ζ which can be used for T or I sections, it is difficult to determine ζ for non-standard structures. In addition to this, there is no formula to compute ζ for the contact between the end surfaces of the structure and the loading platen. Actually, the real effect of the total restraint can be expressed by a restraint factor $k(p)$, where $k(p)$ ranges from zero to infinite (Plaut and Guran, 1994).

When a rectangular elastic isotropic plate is under loading in the x–y plane (Fig. 6), the out-of-plane deflection w can be expressed by the following partial differential equation

$$\frac{\partial^4 w}{\partial x^4} + 2\frac{\partial^4 w}{\partial x^2 \partial y^2} + \frac{\partial^4 w}{\partial y^4} = \frac{1}{D}\left(q + N_x \frac{\partial^2 w}{\partial x^2} + N_y \frac{\partial^2 w}{\partial y^2} + 2N_{xy}\frac{\partial^2 w}{\partial x \partial y}\right) \tag{2}$$

where $w =$ out of plane displacement; $D =$ flexural rigidity of the plate $= \frac{Et^2}{12(1-\upsilon^2)}$; $E =$ Young's modulus; $t =$ Plate thickness; $\upsilon =$ Poisson's ratio; $N_x =$ normal load per unit length in x-direction; $N_y =$ normal load per unit length in y-direction; $N_{xy} =$ shear load per unit length in x–y plane; $q =$ lateral distributed load.

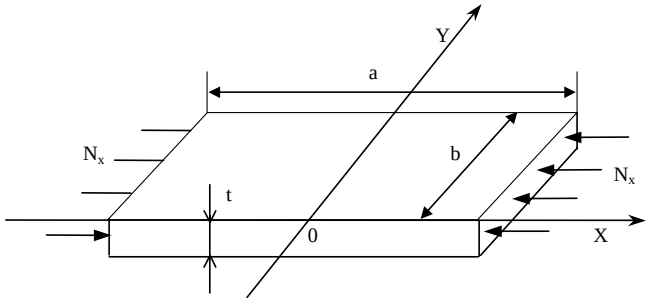

Fig. 6. Rectangular plate under compressive loading.

The plate element (Fig. 6) of the hat section carries uniform in plane compressive load only so that there is only normal load per unit length, N_x, in the direction. Accordingly, letting q, N_y and N_{xy} equal to zero in Eq. (1), we get

$$\frac{\partial^4 w}{\partial \xi^4} + 2R^2 \frac{\partial^4 w}{\partial \xi^2 \partial \eta^2} + R^4 \frac{\partial^4 w}{\partial \eta^4} + \lambda^2 \frac{\partial^2 w}{\partial \xi^2} = 0 \tag{3}$$

where the non-dimensional parameters ξ, η and R are defined as

$$\xi = \frac{x}{a} \quad \eta = \frac{y}{b} \quad R = \frac{a}{b} \tag{4}$$

The plate dimensions a and b are shown in Fig. 6 and the factor λ is defined as

$$\lambda^2 = N_x \frac{a^2}{D} = \sigma_x \frac{12a^2(1-v^2)}{Et^2} \tag{5}$$

The boundary conditions in the non-dimensional form can be written as

for simply supported edges:

$$w = 0; \quad \frac{\partial^2 w}{\partial \eta^2} + \frac{v}{R^2} \frac{\partial^2 w}{\partial \xi^2} = 0 \quad (\eta = 0, 1) \tag{6}$$

for elastically restrained edges:

$$w = 0; \quad \phi = \phi^0 \quad \left(\xi = \pm \frac{1}{2}\right) \tag{7}$$

In Eq. (6), ϕ^0 is the rotation of the loaded edges.

It was stated by Plaut and Guran (1994) that by defining the quantity $k(p)$ as

$$k(p) = \frac{a}{D} K(N_x) = \frac{a}{D} K\left(\frac{\pi^2 D p}{b^2}\right) \tag{8}$$

the elastically restrained boundary condition is

$$\xi = \frac{1}{2}: \quad w = 0; \quad \frac{\partial^2 w}{\partial \xi^2} + k(p) \frac{\partial w}{\partial \xi} = 0 \tag{9a}$$

$$\xi = -\frac{1}{2}: \quad w = 0; \quad \frac{\partial^2 w}{\partial \xi^2} - k(p) \frac{\partial w}{\partial \xi} = 0 \tag{9b}$$

and the linear relationship between $k(p)$ and p is assumed to be of the form

$$k(p) = k_0(1 + \alpha p) \quad k_0 \geqslant 0, \ \alpha \geqslant 0, \ p \geqslant 0 \tag{10}$$

$k(p)$, is then given by the following expression:

$$k(p) = k_0 \left(1 + \frac{\alpha}{(R\pi)^2} \lambda^2\right) \tag{11}$$

The actual buckling mode shape of the plate element is only one half wave length laterally, so we here choose the solution for Eq. (3) as

$$w(\xi, \eta) = F(\xi) \sin(\pi \eta) \tag{12}$$

Obviously, expression (12) automatically satisfies the simply supported boundary condition. Substituting relation (12) in Eq. (3) and considering that $\sin(\pi\eta)$ is not zero, the ordinary differential equation for determining $F(\xi)$ is

$$\frac{d^4F}{d\xi^4} + (\lambda^2 - 2R^2\pi^2)\frac{d^2F}{d\xi^2} + (R\pi)^4F = 0 \tag{13}$$

The general solution for Eq. (13) can be written as

$$F(\xi) = C_1\cos(\alpha_1\xi) + C_2\cos(\alpha_2\xi) + C_3\sin(\alpha_1\xi) + C_4\sin(\alpha_2\xi) \tag{14}$$

where

$$\alpha_1 = \sqrt{\frac{1}{2}(\lambda^2 - 2R^2\pi^2) + \frac{1}{2}\lambda\sqrt{(\lambda^2 - 4R^2\pi^2)}} \tag{15a}$$

$$\alpha_2 = \sqrt{\frac{1}{2}(\lambda^2 - 2R^2\pi^2) - \frac{1}{2}\lambda\sqrt{(\lambda^2 - 4R^2\pi^2)}} \tag{15b}$$

For symmetric buckling mode, both C_3 and C_4 vanish. Using the edge condition (9a) and (9b), we obtain

$$C_1\cos\left(\frac{\alpha_1}{2}\right) + C_2\cos\left(\frac{\alpha_2}{2}\right) = 0 \tag{16a}$$

$$\left(-C_1\alpha_1^2\cos\left(\frac{\alpha_1}{2}\right) - C_2\alpha_2^2\cos\left(\frac{\alpha_2}{2}\right)\right) + k(p)\left(-C_1\alpha_1\sin\left(\frac{\alpha_1}{2}\right) - C_2\alpha_2\sin\left(\frac{\alpha_2}{2}\right)\right) = 0 \tag{16b}$$

For a nontrivial solution, the determinant of the coefficient C_1 and C_2 must vanish, and this leads to the transcendental equation

$$(\alpha_1^2 - \alpha_2^2)\cos\left(\frac{\alpha_1}{2}\right)\cos\left(\frac{\alpha_2}{2}\right) + k(p)\left(\alpha_1\sin\left(\frac{\alpha_1}{2}\right)\cos\left(\frac{\alpha_2}{2}\right) - \alpha_2\cos\left(\frac{\alpha_1}{2}\right)\sin\left(\frac{\alpha_2}{2}\right)\right) = 0 \tag{17}$$

Eq. (17) can be rewritten as

$$(\alpha_1^2 - \alpha_2^2)\cos\left(\frac{\alpha_1}{2}\right)\cos\left(\frac{\alpha_2}{2}\right) = k(p)\left(\alpha_2\cos\left(\frac{\alpha_1}{2}\right)\sin\left(\frac{\alpha_2}{2}\right) - \alpha_1\sin\left(\frac{\alpha_1}{2}\right)\cos\left(\frac{\alpha_2}{2}\right)\right) \tag{18}$$

Eq. (18) can be interpreted graphically by plotting the curve of the left hand side and right hand side of the equation together. The intersecting points are the solutions. Since the number of intersecting points is infinite, only the point that gives the lowest λ value will be of interest. The corresponding value of λ can then be computed numerically.

5. Results and discussion

Fig. 7 shows the deformed specimen at the onset of buckling. It clearly indicates that the two face plate elements (face A and face B) buckled at the same time while both the web plates and the flanges remained straight. Therefore, the face plates should be regarded as the governing plate elements of the hat section structure. During buckling, there was no adhesive bonding separation so that the flange behaved as an integrated plate. The test results for the critical buckling stress are shown in Table 2.

For two values of the spring constant K, the nodal out-of-plane deflections of the common edge between face A and web A, together with those of the longitudinal centerline of face A, are plotted in Figs. 8 and 9 respectively. It can be seen that the deflection level of the common edge is much smaller than that of the centerline, thus, the simply supported boundary condition is appropriate.

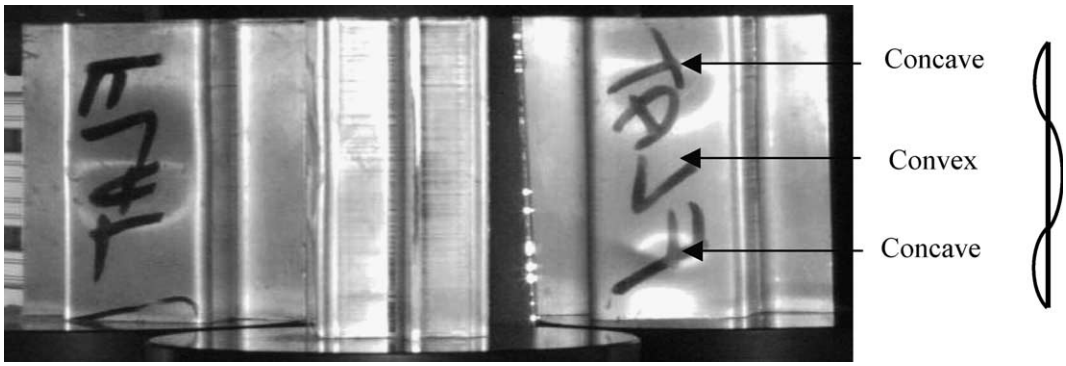

Fig. 7. Buckling deformation of the hat section.

Table 2
Critical buckling stress comparison between analysis and experiment

	α_1	α_2	λ	Analytical result σ_{cr} (MPa)	Difference[a] (%)
$\alpha = 0$					
$k_0 = 0.5$	7.00	5.64	12.64	100.88	10.81
$k_0 = 1.0$	7.31	5.40	12.71	102.00	9.81
$k_0 = 5.0$	8.38	4.71	13.09	108.19	4.34
$k_0 = 10$	8.87	4.45	13.32	112.03	9.46
$k_0 = 100$	9.68	4.08	13.76	119.55	5.70
$k_0 = 0.5$	7.23	5.43	12.70	101.84	9.96
$k_0 = 1.0$	7.62	5.18	12.80	103.45	8.53
$\alpha = 0.2$					
$k_0 = 5.0$	8.85	4.46	13.31	111.86	1.09
$k_0 = 10$	9.25	4.27	13.52	115.42	2.05
$k_0 = 100$	9.92	3.98	13.80	120.25	6.30

[a] Difference from mean experimental result ($\sigma_{cr} = 113.1$ MPa) in percentage.

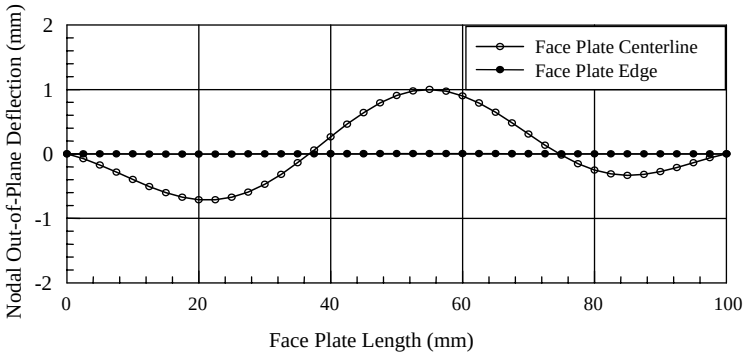

Fig. 8. Finite element result of face plate centerline and common edge out-of-plane deflection $K = 2500$ (N m/rad).

Fig. 10 is a buckled shape comparison between the finite element simulation and the experiment. Since the displacement level at the buckling stage is arbitrary from the finite element simulation and is usually

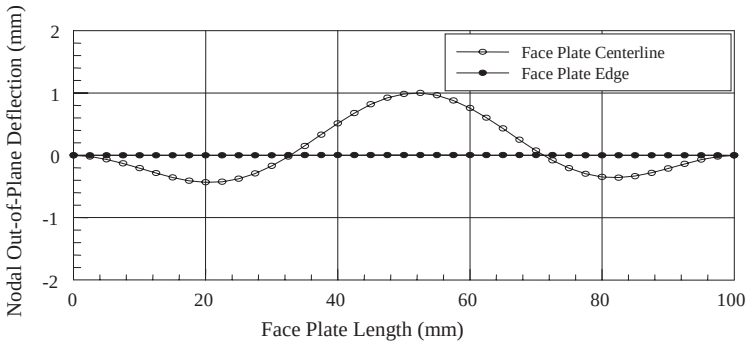

Fig. 9. Finite element result of face plate centerline and common edge out-of-plane deflection $K = 50{,}000$ (N m/rad).

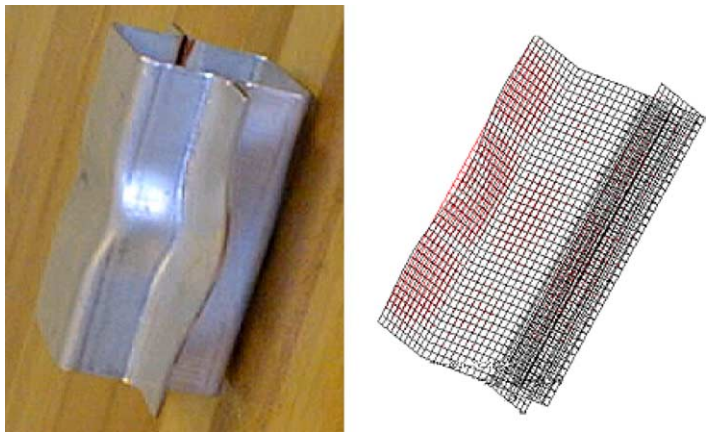

Fig. 10. Buckled shape comparison between the finite element simulation and the experiment.

normalized, it is difficult to correlate them quantitatively. However, the buckled shapes do agree in general. In order to have a clearer view of the buckling deformation about the hat section, the specimen shown in Fig. 10 was purposely compressed a little more so that it underwent some plastic deformation which is just the further development of the initial elastic buckling deformation.

Since the stresses are uniformly distributed on the loading cross section during buckling, with a calculated critical buckling stress value, the critical buckling load can then be found. Table 2 shows the comparison between the analytical and experimental buckling stresses. It shows that the combination of $k_0 = 5$ and $\alpha = 0.2$ yields the buckling load value that is the closest to that gained from the tests.

Since p is directly proportional to the normal load N_x, k_0 in Eq. (10) represents the combined structural elastic restraint effect on the face plate from other stiffening plate members when $N_x = 0$. This combined structural elastic restraint usually refers to the rotational restraint from the side plate members such as the web plate and flanges. The elastic restraint effect from the loading is then taken into account by the factor α in Eq. (10), which magnifies the normal load contribution to the restraint effect.

Even though $k_0 = 5$ and $\alpha = 0.2$ yield the buckling load value that is the closest to the measured value, there is no particular physical meaning to these two specific numerical values. They simply stem from applying the equation to the results of a particular experiment.

6. Conclusions

Adhesively bonded hat sections experience symmetric buckling deformations under axial compression. There is no adhesive or cohesive failure at buckling stage so that the flange behaves as an integrated plate that is thicker than the face plate. Finite element analysis can be employed to verify the boundary conditions of some specific edges in the non-standard structures. The theoretical method based on the partial differential equation can give satisfactory result. With the calculated critical buckling stress, the buckling load can be obtained by simply multiplying the stress by the cross section area of the structure.

Acknowledgments

The authors gratefully acknowledge the financial support from the Ford Motor Company and the technical assistance of Carl Johnson, Matt Zaluzec, John Hill, Kim Lazarz and Jenny Wang of the Ford Scientific Research Laboratory.

References

ABAQUS/Standard User's Manual, 1998. Version 5.8, Hibbitt, Karlsson and Sorensen, Inc.

Bao, G., Jiang, W., Roberts, J.C., 1997. Analytic and finite element solutions for bending and buckling of orthotropic rectangular plates. International Journal of Solids and Structures 34 (14), 1797–1822.

Becker, H., 1957. Buckling of comp. elements—Part II. Handbook of Structural Stability. National Advisory Committee for Aeronautics, NACA TN 3782.

Bleich, F., 1952a. Buckling Strength of Metal Structures. McGraw-Hill Book Company Inc.

Bleich, F., 1952b. Buckling Strength of Metal Structures. McGraw-Hill Book Company Inc., pp. 433–436.

Bulson, P.S., 1969a. The Stability of Flat Plates. American Elsevier Publishing Company, Inc.

Bulson, P.S., 1969b. The Stability of Flat Plates. American Elsevier Publishing Company, Inc., p. 295.

Gan, L.H., Ye, L., Mai, Y.W., 1999. Simulations of mechanical performance of pultruded I-beam with various flange-web conjunctions. Composites Part B: Engineering 30 (4), 423–429.

Paik, J.K., Thayamballi, A.K., 2000. Buckling strength of steel plating with elastically restrained edges. Thin-Walled Structures 37, 27–55.

Peery, D.J., 1949. Aircraft Structures. McGraw-Hill Book Company, Inc, p. 373.

Plaut, R.H., Guran, A., 1994. Buckling of plates with stiffening elastically restrained edges. Journal of Engineering Mechanics—ASCE 120 (2), 408–411.

Saint Venant, 1883. Discussion in "Theorie de l'elasticite des corps solids", by Clebsch, p. 704.

Timoshenko, S., 1961a. Theory of Elastic Stability. McGraw-Hill Book Company, Inc., New York, p. 411.

Timoshenko, S., 1961b. Theory of Elastic Stability. McGraw-Hill Book Company, Inc., New York, p. 356.